Graphical Solution of the Material Balance Constraint for MSMPR Crystallizers

E. T. White and A. D. Randolph
Department of Chemical Engineering
University of Arizona
Tucson, AZ 85721

This note shows how the material balance constraint may be incorporated into the semilog plotting method for mixed-suspension, mixed-product-removal (MSMPR) crystallizers.

MSMPR Theory

The analysis of the unseeded continuous mixed-suspension, mixed-product-removal crystallizer with size-independent growth leads to an exponential crystal size distribution (CSD) (Randolph and Larson, 1971).

In terms of population density $n(L)$ and particle size L, this is expressed as:

$$n(L) = n^\circ \exp(-L/\bar{L}) \tag{1}$$

where the mean size $\bar{L} = G\tau$ is the product of the growth rate G and the mean residence time τ. The nuclei population density n° equals B°/G, where B° is the nucleation rate.

Alternatively, the distribution can be expressed in terms of the cumulative number oversize distribution, $N(L)$, given by:

$$N(L) = N^\circ \exp(-L/\bar{L}) \tag{2}$$

where $N^\circ = B^\circ\tau$ is the total number of crystals.

The material balance relation links the parameters of the above distribution to the suspension density, M_T, by:

$$M_T/6\rho_c k_v = \mu_3 = n^\circ(G\tau)^4 = N^\circ(G\tau)^3 \tag{3}$$

where ρ_c is the crystal density, k_v the volumetric shape factor, and μ_3 the unnormalized third moment of the distribution.

Strictly, the term "material balance relation" applies when the suspension density is related to the change between inlet and outlet solution concentrations. The above relation is really a self-consistency check; it tests that the measured quantities satisfy the third moment for the expected exponential distribution. The last two equalities in Eq. 3 result from the direct integration of the distribution of Eq. 1.

Plotting of Experimental Data

The CSD from an MSMPR crystallizer is plotted on semilog paper either as the population density, Eq. 1, or as the cumulative number oversize, Eq. 2. A straight line results, with slope equal to $-1/\bar{L} = -1/G\tau$ and intercept as either n° or N°. The best estimates of slope and intercept are found either by eye or by linear regression; however, these values seldom satisfy Eq. 3 with an acceptable accuracy. Usually the estimates of the intercept and $\bar{L}$ are then adjusted to satisfy this equation. Often the estimate of $\bar{L}$ is unaltered and a new intercept is chosen satisfying Eq. 3, since the intercept obtained from the semilog plot has the larger uncertainty.

Such a procedure means that the value of the slope usually will not be the best estimate simultaneously satisfying Eq. 3 and Eq. 1 (or Eq. 2). Further, any error in the estimate of $\bar{L}$ will, by satisfying Eq. 3, give a complementary error in B°. That is, the estimate of B° is correlated with the estimate of G, according to $B^\circ \propto G^{-3}$. Figure 1 shows the results of several independent estimates of the slope of the semilog plot of Figure 2 and the corresponding value of B° from Eq. 3. The -3 power dependence is obvious. A similar trend would result from repeated CSD measurements at fixed operating conditions. Also shown in Figure 1 is a second set of values for operation at twice the residence time. Again the -3 dependence is apparent.

Such results are frequently obtained from industrial crystallizers, which of necessity operate at a near-constant mean residence time. From data at a fixed residence time, one might conclude erroneously that the nucleation rate decreases as the supersaturation, as represented by G, increases. It cannot be too strongly emphasized that this apparent trend is solely the result of experimental errors compounded with Eq. 3. The true dependence of B° on G can only be evaluated when a substantial change in operating growth rate is made, as shown by the two

E. T. White is on leave from the Department of Chemical Engineering, University of Queensland, Brisbane, Australia 4067.

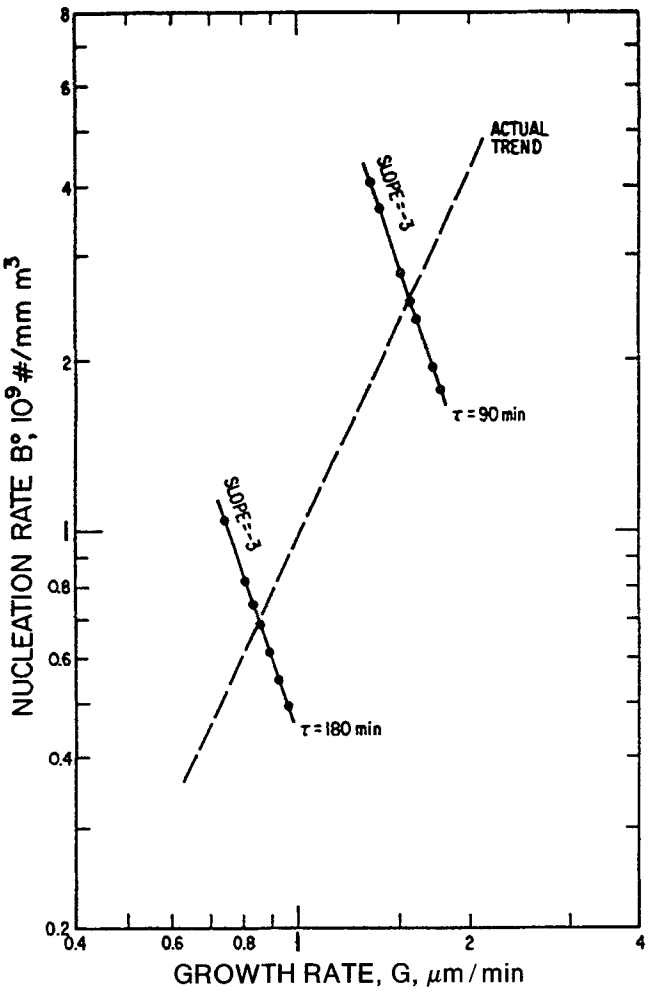

Figure 1. Effect of errors in estimation of growth rate on nucleation rate.

sets of data in Figure 1. This is usually achieved by manipulation of the residence time over a fairly broad range, as previously pointed out by Keight (1978). However, better estimates of B° and G can be obtained if both the size distribution relation and the self-consistency check are solved simultaneously.

Simultaneous Solutions of Equations

Population density form

Equations 1 and 3 may be solved simultaneously to give:

$$y \equiv \ln\left(n(L)\rho_c k_v/M_T\right) = L/\bar{L} - 4\ln\bar{L} - \ln 6 \qquad (4)$$

This equation satisfies both the exponential size distribution and the self-consistency check. It has only one parameter, $\bar{L}$. As $\bar{L}$ varies, it generates a family of straight lines with slope $-1/\bar{L}$ and intercept $(-4\ln\bar{L} - \ln 6)$.

This family of straight lines is tangential to a locus curve. The differential equation for this curve is obtained by substituting:

$$\frac{dy}{dL} = -1/\bar{L} \qquad (5)$$

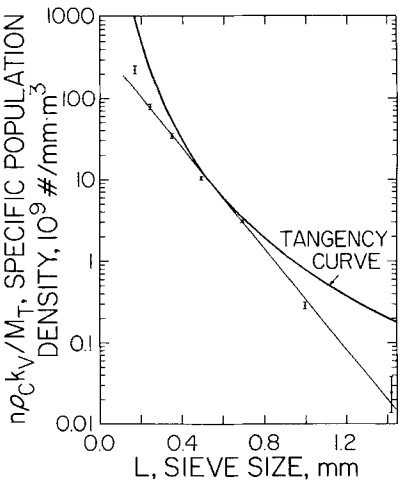

Figure 2. Tangency curve for population density semilog plot.
Specific population density, $n\rho_c k_v/M_T$ used; data for a Glauber's salt MSMPR crystallization are shown

in Eq. 4 to give:

$$y = L\frac{dy}{dL} + 4\ln\left(-\frac{dy}{dL}\right) - \ln 6 \qquad (6)$$

which has the solution:

$$n(L)\rho_c k_v/M_T = \beta_1 L^{-4} \qquad (7)$$

where $\beta_1 = 4^4 \exp(-4)/6 = 0.7815$.

This curve, termed the tangency curve, is plotted in Figure 2. A straight line drawn as a tangent to this curve will satisfy the self-consistency relation, Eq. 3. Thus the best estimate of $\bar{L}$ for MSMPR data will be that tangent giving the closest fit to the experimental points. Once the best estimate of $\bar{L}$ is obtained, n° is obtained from Eq. 3. The point of tangency is at $L = 4\bar{L}$, but this is not an accurate estimate of $\bar{L}$.

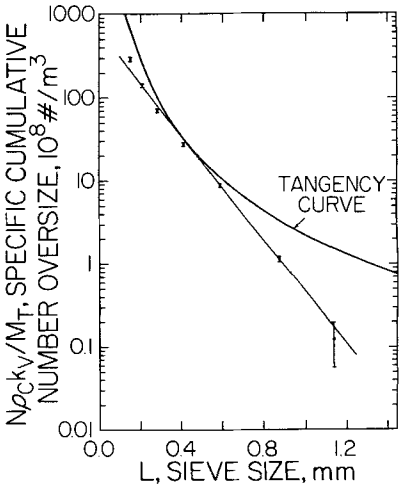

Figure 3. Tangency curve for cumulative number oversize semilog plot.
Data for same run as Figure 2

Figure 2 plots the log of $n(L)\rho_c k_v/M_T$ (which we have called the specific population density), rather than log n. In this form the plot is completely general and will apply for all measurements on all MSMPR systems. In fact, the evaluation of the specific population density requires less computation than does n. Indeed, ρ_c, k_v, and M_T need not be known and the plot can still be used.

If the traditional plot form involving log n is used, the tangency curve is specific to the material being crystallized (ρ_c, k_v) and the operating conditions (M_T). As these change, different tangency curves will have to be drawn. Values of $n(L)\rho_c k_v/M_T$ for the tangency curve can be generated from Eq. 1.

To illustrate the method, the Appendix shows data for the MSMPR crystallization of Glauber's salt, $Na_2SO_4 \cdot 10H_2O$. These are the results shown in Figure 2. Estimates of $\bar{L}$ are given in the Appendix.

Cumulative number oversize form

In a similar manner, Eq. 3 may be substituted into Eq. 2 to give Eq. 8, which satisfies both the cumulative number exponential distribution and the self-consistency check, as:

$$Y \equiv \ln (N\rho_c k_v/M_T) = -L/\bar{L} - 3 \ln \bar{L} - \ln 6 \qquad (8)$$

Again this represents a family of straight lines that can be shown to be tangent to:

$$N\rho_c k_v/M_T = \beta_2 L^{-3} \qquad (9)$$

where $\beta_2 = 3^3 \exp(-3)/6 = 0.2240$.

The point of tangency is now at $L = 3\bar{L}$. Figure 3 shows the tangency curve in this form with experimental points plotted for the same data as Figure 2.

Discussion

A more accurate estimate of the crystallization kinetic parameters will result for MSMPR data if the self-consistency check is solved simultaneously with the exponential size distribution. This can be carried out graphically if the tangency curve is drawn on semilog paper and the straight line estimate is chosen as a tangent to this curve. Using specific pouplation densities, $n\rho_c k_v/M_T$, or specific cumulative number oversize, $N\rho_c k_v/M_T$, generalized graph paper can be prepared that is directly applicable to all MSMPR crystallization results.

If a numerical, rather than a graphical technique is to be used, $\bar{L}$ may be chosen to minimize y in Eq. 4 or Y in Eq. 8. This requires a one-parameter optimization routine, where the objective function could be a weighted least-squares criterion. The usual linear regression least-squares estimation of $\bar{L}$ could be used as a starting value. Values obtained on the data of Figure 2 by such a technique are also given in the Appendix.

An estimate of $\bar{L}$ can also be obtained directly from the cumulative mass distribution. For MSMPR crystallizer operation, the cumulative mass distribution, F, is given by a third-order gamma distribution (Randolph and Larson, 1971):

$$F(L) = 1 - (1 + x + x^2/2 + x^3/6)e^{-x} \qquad (10)$$

where $x = L/\bar{L}$.

Figure 4 shows third-order gamma graph paper drawn up so that the ordinate is scaled according to Eq. 10 (after Nyvlt, 1982); the data from the Appendix are plotted. If the MSMPR assumptions hold, a straight line results. Since the median (50%) point corresponds to 3.67 $\bar{L}$, a value of $\bar{L}$ and thus G and B° can be obtained. Error bars are shown. While such plots are very convenient, care should be taken not to overemphasize outlying points, which have considerable errors. Note that such a plot can only be used if the MSMPR assumptions are satisfied in full.

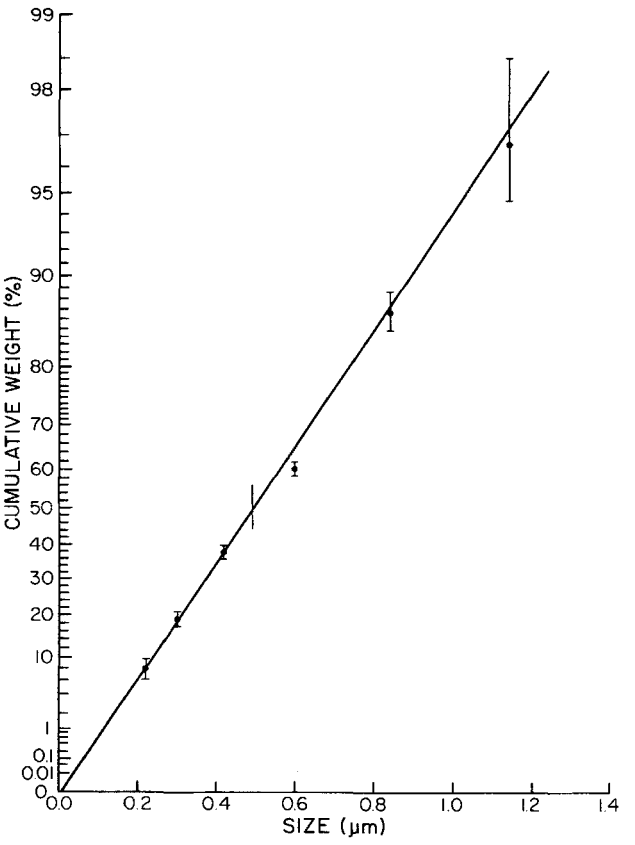

Figure 4. Cumulative mass plot on third-order gamma paper.
A straight line should result if the MSMPR assumptions apply; data for same run as Figure 2

Table 1. Sieve Analysis for Glauber's Salt Crystallization

Sieve Aperture mm	Mid Size mm	% Mass on Sieve	Cumul. % Mass	Specif. Pop. Dens. 10^9#/mm · m^3	Specif. Cum. No. 10^9#/m^3
	1.414	3.4		0.024	
1.189			96.6		0.012
	1.000	10.0		0.29	
0.841			86.6		0.112
	0.707	26.6		3.1	
0.595			60.0		0.86
	0.500	22.7		10.4	
0.420			37.3		2.68
	0.354	18.7		34	
0.297			18.6		6.9
	0.250	10.8		79	
0.210			7.8		13.8
	0.177	7.8		229	
0.149			0.0		27.9

11 L crystallizer $\tau = 90$ min, $\rho k_v = 810$ kg/m^3, $M_T = 300$ kg/m^3

Conclusion

The exponential size distribution and the material balance relation (self-consistency check) can be solved simultaneously on a semilog plot by selecting the tangent to the tangency curve that best fits the experimental data.

Appendix. Example of Treatment of MSMPR Results

Table 1 shows a sieve analysis obtained at steady state from the crystallization of Glauber's salt ($Na_2SO_4 \cdot 10H_2O$) from aqueous solution in an 11 L laboratory MSMPR crystallizer.

The mid sieve size, L_i, is taken as the geometric mean of bounding sieves. For the end sieves, it is assumed that all material would be retained in the next sieve function. The specific population density is given by:

$$n\rho_c k_v / M_T = \omega_i / \Delta L \, L_i^3 \, \Sigma\omega_i \tag{A1}$$

and the increment in specific cumulative number by:

$$\Delta N \rho_c k_v / M_T = \omega_i / L_i^3 \, \Sigma\omega_i \tag{A2}$$

where ω_i is the mass on sieve i.

Considering the righthand sides of these equations, it can be seen that values of $\rho_c k_v$, or M_T are not required in order to evaluate the specific quantities. This is a result of Eq. 3 being a self-consistency check rather than a strict material balance relation.

The specific cumulative number oversize can be obtained by summing the increments. Table 1 shows the computed values. The results have been plotted in Figures 2, 3, and 4. The population density is plotted against the mean size and the cumulative number and cumulative mass against the retaining sieve size.

On each figure, the tangent most closely fitting the data has been selected visually, giving estimates of $\bar{L}$ of 0.140 and 0.145 mm, respectively. The corresponding values found by a numerical optimization procedure using either Eq. 4 or Eq. 8 with a weighted least-squares objective function was 0.139 mm. The estimated 95% uncertainty on these estimates is about ±20%.

The cumulative mass data were plotted directly on Figure 4. A reasonable straight line results. From the 50% size, $\bar{L}$ was estimated as 0.135 mm, ±20%.

Error bars on the figures are based on an assumed error of ±1.0 on each of the interior mass percentage observations and ±2.0 for the end sieves. This data-fitting technique implies nothing as to the absolute accuracy of the screen analysis, merely that the estimated value of $\bar{L}$ is consistent.

If a number-counting particle size analyzer had been used, giving a size distribution as the number of particles, Δ_i in channel i, the equations corresponding to Eqs. A1 and A2 are:

$$n\rho_c k_v / M_T = \Delta_i / \Sigma(\Delta_i L_i^3) \Delta L \tag{A3}$$

$$\Delta N \rho_c k_v / M_T = \Delta_i / \Sigma(\Delta_i L_i^3) \tag{A4}$$

Again, for the specific distribution quantities, values of ρ_c, k_v and M_T are not required, as the righthand sides of the equations depend only on the size analysis.

Literature cited

Keight, D. V., Comments on "An Investigation into the Nucleation Kinetics of Urea Crystallization in Water by Means of Crystal-Size Distribution Analysis," *Ind. Eng. Chem. Process Des. Dev.*, **17**(4), 576 (1978).

Nyvlt, J., *Industrial Crystallization—State of the Art*, 2nd ed., Weinkim Verlag, 19 (1982).

Randolph, A. D., and M. A. Larson, *Theory of Particulate Processes*, Academic Press, New York 68 (1971).

Manuscript received June 3, 1986, and revision received Sept. 5, 1986.